

Tectonic evolution of the Pacific margin of Antarctica

2. Structure of Late Cretaceous–early Tertiary plate boundaries in the Bellingshausen Sea from seismic reflection and gravity data

Alex P. Cunningham,¹ Robert D. Larter, and Peter F. Barker

British Antarctic Survey, Natural Environment Research Council, Cambridge, England, UK

Karsten Gohl and Frank O. Nitsche²

Alfred Wegener Institute for Polar and Marine Research, Bremerhaven, Germany

Received 27 March 2002; revised 13 April 2002; accepted 9 May 2002; published 13 December 2002.

[1] Interpretations of multichannel seismic (MCS) reflection and potential field data suggest that some prominent gravity anomalies in the Bellingshausen Sea are associated with plate boundaries that were active during the Late Cretaceous and early Tertiary. Between 83° and 93°W, a belt of negative anomalies extends along the West Antarctic continental slope, which we term the continental slope gravity anomaly (CSGA). MCS profiles show that the CSGA coincides with an acoustically opaque structural high imaged beneath the lower slope. We interpret this structure as the upper part of an accretionary prism which formed during southward subduction of the Phoenix and Charcot plates, before Chatham Rise separated from West Antarctica. MCS profiles crossing the same margin to the northeast show no evidence of an extensive buried accretionary prism, but instead reveal an abrupt northeastward steepening of the continental slope near 78°W. We attribute this change in tectonic style, at least in part, to subduction erosion resulting from subduction of rough oceanic basement which formed at the Antarctic-Phoenix ridge after an abrupt decrease in spreading rate at chron 23r (52 Ma). Near 95°W, the Bellingshausen gravity anomaly (BGA) consists of a prominent low-high gravity couple which crosses the West Antarctic continental shelf, slope, and rise. The BGA corresponds to a buried asymmetric basement trough, where Cretaceous oceanic basement dips beneath more elevated basement to the east. The trough probably formed after subduction of Charcot plate ocean floor stalled at the nearby Antarctic Peninsula margin, near the end of the Cretaceous Normal Superchron. Ocean floor to the east of the BGA became attached to the Antarctic Peninsula, and the BGA trough subsequently accommodated a small amount of convergent motion between the Antarctic Peninsula and the ocean floor to the west (initially part of the Marie Byrd Land plate and later part of the Bellingshausen plate). Tectonism probably ceased at the BGA at chron 27 (61 Ma), as a result of a general plate reorganization in the South Pacific. *INDEX TERMS*: 3010

Marine Geology and Geophysics: Gravity; 3025 Marine Geology and Geophysics: Marine seismics (0935); 3040 Marine Geology and Geophysics: Plate tectonics (8150, 8155, 8157, 8158); *KEYWORDS*: Antarctic, Pacific, Bellingshausen Sea, Cretaceous, Tertiary, continental margin

Citation: Cunningham, A. P., R. D. Larter, P. F. Barker, K. Gohl, and F. O. Nitsche, Tectonic evolution of the Pacific margin of Antarctica, 2. Structure of Late Cretaceous–early Tertiary plate boundaries in the Bellingshausen Sea from seismic reflection and gravity data, *J. Geophys. Res.*, 107(B12), 2346, doi:10.1029/2002JB001897, 2002.

1. Introduction

[2] In recent years, marine gravity fields derived from satellite altimetry data [McAdoo and Marks, 1992; McAdoo and Laxon, 1997; Sandwell and Smith, 1997] have led to major advances in Antarctic tectonic reconstruction. These

data describe seafloor morphology and tectonic fabric in remote parts of the Southern Ocean where geophysical ship tracks are sparse, and have been used to design surveys in key areas of the South Pacific. One such region is the Bellingshausen Sea, which lies north of Ellsworth Land, West Antarctica (Figure 1). There, satellite gravity data revealed three prominent anomalies on the Antarctic continental rise: the “Bellingshausen gravity anomaly” (BGA), extending north-northeast from the West Antarctic continental margin near 95°W to c. 68°S; the “continental slope gravity anomaly” (CSGA), a belt of negative anomalies along the lower continental slope between 83 and 93°W; and the “De Gerl-

¹Now at ARK CLS Limited, Milton Keynes, UK.

²Now at Lamont-Doherty Earth Observatory of Columbia University, Palisades, New York, USA.

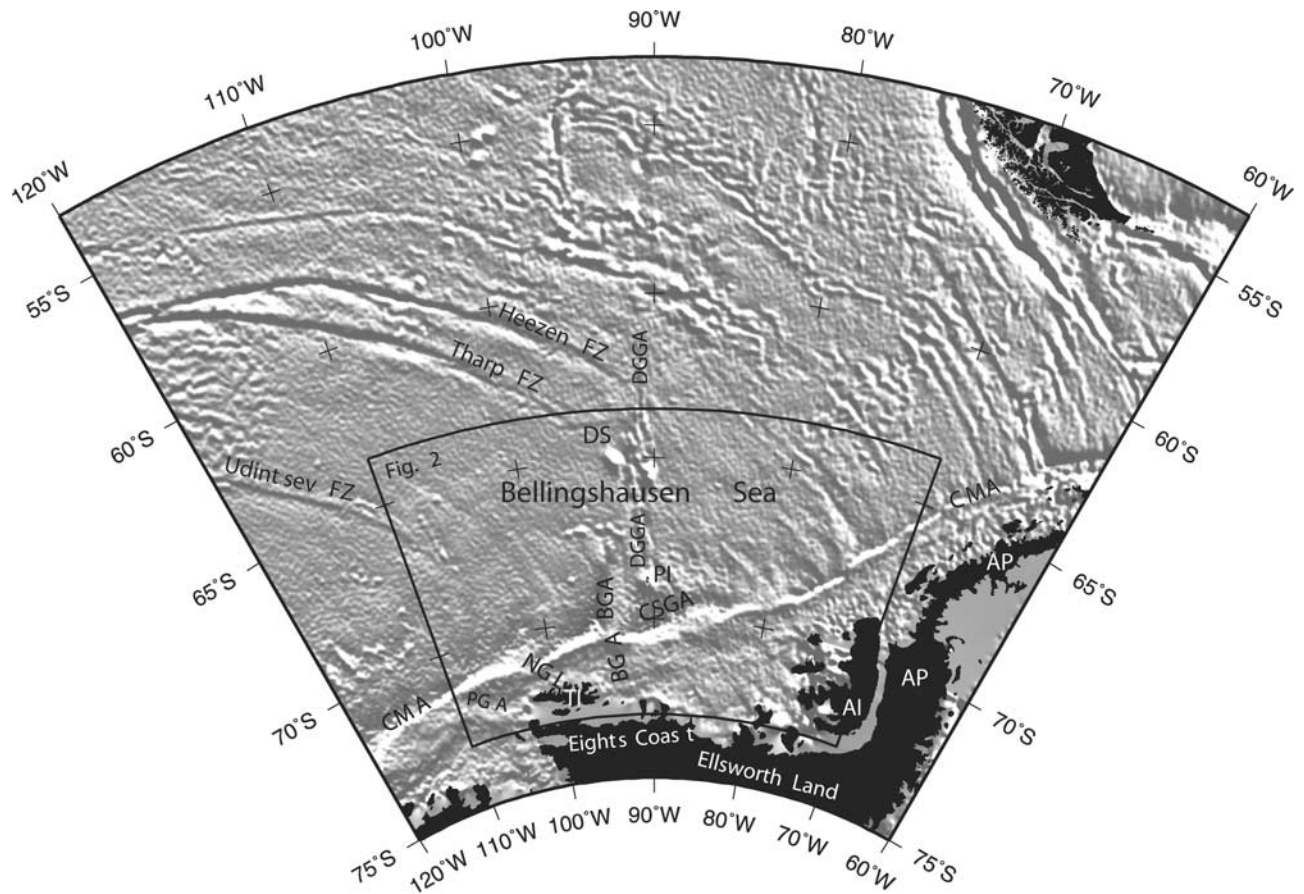


Figure 1. Shaded relief grayscale display of the free-air gravity field in the southeast Pacific derived from satellite altimetry data (illuminated from the northeast: north of 70°S [Sandwell and Smith, 1997], south of 70°S [McAdoo and Laxon, 1997]). Positive free-air anomalies and northeast-dipping gradients appear light, and negative anomalies and southwest-dipping gradients appear dark. Major FZ anomalies are labeled, and the area shown in Figure 2 is outlined. BGA, Bellingshausen gravity anomaly; CSGA, continental slope gravity anomaly; DGGGA, De Gerlache gravity anomaly; PGA, Peacock gravity anomaly [Larter *et al.*, 2002]; NGL, Noville gravity lineation [Larter *et al.*, 2002]; CMA, continental margin anomaly; DS, De Gerlache Seamounts; AI, Alexander Island; AP, Antarctic Peninsula; TI, Thurston Island; PI, Peter I Island.

ache gravity anomaly” (DGGGA), a linear anomaly with a central high and flanking lows, which extends from Peter I Island to 62°S (all located in Figures 1 and 2a).

1.1. Tectonic Framework

[3] Although the Bellingshausen Sea now lies entirely within the Antarctic plate, tectonic reconstructions show

that it has a complex history involving several plates [Mayer *et al.*, 1990; McCarron and Larter, 1998]. In particular, marine magnetic data show two principal tectonic provinces on the continental rise north of Marie Byrd Land and Ellsworth Land: a western province where magnetic anomalies record seafloor spreading in the wake of Chatham Rise as it migrated north-westward following its separation from

Figure 2. (opposite) (a) MCS profile tracks in the Bellingshausen Sea plotted on satellite-derived marine gravity data (north of 70°S [Sandwell and Smith, 1997], south of 70°S [McAdoo and Laxon, 1997], shaded relief as for Figure 1). MCS tracks are marked with thin black lines, and interpreted line drawings shown in this study (Figures 3a–3i) are located with bold black line segments. DSDP and ODP drill sites are marked with solid triangles. PGA, Peacock gravity anomaly; NGL, Noville gravity lineation; TI, Thurston Island; AI, Alexander Island; BGA, Bellingshausen gravity anomaly; CSGA, continental slope gravity anomaly; DGGGA, De Gerlache gravity anomaly; CMA, continental margin anomaly. (b) Magnetic isochrons (bold black bars with italicized labels) and FZ lineaments (bold dotted lines) determined from marine gravity and magnetic data [Larter *et al.*, 2002]. Selected free-air gravity anomaly contours from McAdoo and Laxon [1997] are plotted at 25 mGal intervals (except 0 mGal contour); –25 mGal contours surrounding the BGA minimum, the CSGA and the DGGGA are marked with bold lines. Solid gray ornament locates anomalies associated with Peter I Island and two volcanic guyots of the De Gerlache seamount group. Red horizontal ornament locates oceanic basement formed at the PAC-MBL/PAC-BEL ridge; blue crossed ornament locates oceanic basement formed at the Antarctic-Phoenix (ANT-PHO) ridge; green vertical ornament locates oceanic basement of unknown age and origin.

Pleistocene volcano located at the southern terminus of the DGGGA [Prestvik *et al.*, 1990], and the De Gerlache seamounts (Figures 1 and 2), a more northerly volcanic seamount group near the same gravity anomaly. Alkali basalts dredged from the two largest De Gerlache seamounts have yielded early Miocene Ar/Ar and K/Ar ages [Hagen *et al.*, 1998; British Antarctic Survey, unpublished data].

[5] Previous reconstructions have attempted to describe Bellingshausen Sea tectonic evolution since the separation of New Zealand from West Antarctica [Molnar *et al.*, 1975; Herron and Tucholke, 1976; Weissel *et al.*, 1977; Cande *et al.*, 1982; Stock and Molnar, 1987; Mayes *et al.*, 1990; McCarron and Larter, 1998]. In this study, we refer to new tectonic reconstructions in our companion paper [Larter *et al.*, 2002]. These new reconstructions describe Late Cretaceous Bellingshausen Sea tectonic evolution in unprecedented detail, and our interpretations should be followed with reference to this updated tectonic history. Ages quoted for magnetic reversal chrons throughout this paper are from Cande and Kent [1995].

1.2. Objectives of This Study

[6] Several previous studies based on seismic reflection data from the Bellingshausen Sea focus on glacial continental margin sedimentation [Tucholke and Houtz, 1976; Tucholke, 1977; Cunningham *et al.*, 1994; Nitsche *et al.*, 1997, 2000]. However, tectonic evolution has been described by Kimura [1982], Gohl *et al.* [1997a, 1997b], Larter *et al.* [1999], and Cunningham *et al.* [2002]. In this paper, we present interpretations of multichannel seismic reflection (MCS) profiles and gravity data collected by the British Antarctic Survey (BAS) and the Alfred Wegener Institute for Polar and Marine Research (AWI). Our main objectives are:

1. To describe the origin of the BGA and CSGA. We describe the tectonic structures which generate these anomalies, and explain their origin in terms of our new tectonic framework [Larter *et al.*, 2002].

2. To determine the mechanism of deformation at the BGA. Previous workers have suggested that deformation in the vicinity of the BGA resulted either from early Tertiary transpressional motion between the Bellingshausen and Phoenix plates [Gohl *et al.*, 1997a], or from intraplate deformation [McAdoo and Laxon, 1997]. We evaluate these conflicting hypotheses in the light of our updated tectonic framework, and conclude that it probably resulted from Late Cretaceous to early Tertiary convergence between the Bellingshausen plate, and the plate, or plates, comprising West Antarctica.

3. To account for variations in the tectonic style and slope morphology of the West Antarctic continental margin. In particular, we identify continental margin deformation close to the BGA, and a thick, deformed sediment wedge beneath the lower continental slope east of the BGA which coincides with the CSGA.

2. Data Analysis

[7] In 1993, 1994, and 1995, BAS and AWI collected MCS profiles over the BGA, DGGGA, CSGA, and the nearby West Antarctic continental margin (Figure 2a). We also collected “Hydrosweep” swath bathymetry (on AWI

tracks), 3.5 kHz and “Parasound” subbottom profiles, gravity and magnetic data, and dredged rock samples from the De Gerlache seamounts.

2.1. Regional Gravity Data

[8] Free-air gravity fields derived from satellite altimetry data [McAdoo and Marks, 1992; McAdoo and Laxon, 1997; Sandwell and Smith, 1997] show that the BGA is a low-high gravity couple (contrast > 100 mGal) which trends north-northeast across the West Antarctic continental rise between 93 and 96°W (Figures 1 and 2a). It corresponds to the western branch of the “De Gerlache-Peter I Island lineation” of McAdoo and Laxon [1997]. The northern part of the BGA extends from the West Antarctic margin to c. 68°S, where its positive and negative components are separated by a steep (>5 mGal km⁻¹) westward dipping gravity gradient (e.g., at 70°S, 94°45'W, Figure 2a). Farther south, the BGA crosses the continental margin, and trends NNW-SSE across the continental shelf northeast of Thurston Island (Figure 2a). Here, the BGA has a shallower westward gradient (c. 2.5 mGal km⁻¹ near MCS profile BAS923-26, Figure 2a).

[9] The DGGGA extends northward from Peter I Island to about 62°S (Figures 1 and 2a), and along much of its length consists of a central free-air gravity high with flanking lows (contrast locally >50 mGal). Near 65°S, the DGGGA separates two gravity highs corresponding to guyots of the De Gerlache seamount group [Hagen *et al.*, 1998] (Figures 1 and 2). A large positive anomaly is also centered on Peter I Island (68°50'S, 90°30'W). The CSGA consists of a belt of negative anomalies (minimum < -75 mGal) which extends along the lower continental slope between 83 and 93°W (Figures 1 and 2).

[10] The continental shelf edge is marked by the continental margin anomaly (CMA), a chain of gravity highs with steep gradients on their seaward flanks (Figures 1 and 2a). The outer shelf south of the CSGA has a wider than normal CMA, particularly west of 87°W (Figure 2a).

[11] Satellite-derived gravity data and magnetic anomalies (described below) define the Udintsev, Tharp, and Heezen fracture zones (FZs, Figure 1), and more subtle FZ lineations (Figure 2b). All Bellingshausen Sea FZ anomalies have consistent northwest-southeast alignments. The Udintsev FZ can be traced southeastward to c. 67°30'S where its expression fades. Farther northeast, the Tharp and Heezen FZs can be traced southeastward to the DGGGA. The Tharp FZ meets the DGGGA near the De Gerlache seamounts (65°S, Figures 1 and 2a), and the Heezen FZ meets the DGGGA near 63°S (Figure 1). Directly east of the DGGGA, FZ gravity anomalies are very subdued, and FZ trends have been inferred largely from marine magnetic data (Figure 2b). Although some FZ anomalies identified on opposing sides of the DGGGA are colinear, gravity data do not demonstrate FZ continuity across this feature.

2.2. Regional Magnetic Data

[12] Larter *et al.* [2002] present new marine magnetic profiles with published data [Herron and Tucholke, 1976; Kimura, 1982; Larter and Barker, 1991a; Larter *et al.*, 1999; National Geophysical Data Center, 1996], and show that the BGA, DGGGA, and CSGA lie in an area which separates two distinct tectonic provinces: magnetic anomalies to the west record the northwestward migration of the

Pacific-Marie Byrd Land/Pacific-Bellingshausen (PAC-MBL/PAC-BEL) ridge following the rifting of Chatham Rise from West Antarctica (oceanic basement marked with a red ornament, Figure 2b) whereas anomalies to the east record the southeastward migration of the ANT-PHO ridge toward the Antarctic Peninsula (blue ornament, Figure 2b). However, the age and origin of an intervening area of ocean floor remain uncertain (green ornament, Figure 2b). Marine magnetic anomalies provide important constraints on the regional tectonic evolution, and on the maximum age of sediments observed on seismic profiles on the continental rise.

2.3. Multichannel Seismic Reflection Data

[13] BAS and AWI MCS profiles are located in Figure 2a. BAS profiles were acquired during RRS *James Clark Ross* cruise JR04 (1993), using an air gun source (total chamber capacity = 55.9 l) and a seismic streamer with an active length of 2400 m (48 × 50 m hydrophone groups). AWI profiles were collected during R/V *Polarstern* cruises ANT-XI/3 (1994) and ANT-XII/4 (1995), using air gun (total chamber capacity = 24 l) and GI gun (total chamber capacity = 13.5 l) sources, and seismic streamers with active lengths of 2400 and 600 m (96 × 25 m and 96 × 6.25 m groups, respectively).

2.3.1. AWI-94002

[14] Profile AWI-94002 (along 292°, Figures 2a and 3a) crosses the continental shelf edge near 75°30'W. An ANT-PHO ridge segment migrated to this part of the margin at about chron 11r (30 Ma) [Larter *et al.*, 1997].

[15] Southeast of common-midpoint (CMP) 4075 (Figure 3a), AWI-94002 shows a prograded sediment wedge beneath the outer shelf [Nitsche *et al.*, 1997, 2000]. Two prominent reflections beneath the shelf (e.g., at 1.4 s two-way-time (TWT) near CMP 2900, Figure 3a) and upper slope (e.g., at 2.4 s TWT near CMP 4150, Figure 3a) might correspond to the base of the wedge.

[16] Northwest of CMP 4075, AWI-94002 crosses the continental slope (gradient $\leq 13^\circ$) and rise. Here, the top of oceanic basement appears fairly smooth (e.g., at 5–7 s TWT, northwest of c. CMP 4675, Figure 3a) with the exception of an isolated high near CMP 5275. At shallower depth, rise sediments show a submarine channel-and-mound depositional system (Figure 3a). Similar depositional systems are observed on profiles AWI-94003, AWI-94040, BAS923-27, BAS923-25, AWI-94042, and BAS923-24 (Figure 3). The irregular seafloor imaged between CMPS 4800 and 7400 (Figure 3a) corresponds to the eroded flank of a sediment drift [Nitsche *et al.*, 2000].

2.3.2. AWI-94003

[17] Profile AWI-94003 (along 167°, Figures 2a and 3b) crosses the shelf edge near 80°W. An ANT-PHO ridge segment migrated to this part of the margin 44–40 Ma ago [McCarron and Larter, 1998].

[18] Southeast of CMP 9400 (Figure 3b), AWI-94003 shows an aggraded/prograded sediment wedge beneath the outer shelf [Nitsche *et al.*, 1997, 2000]. A prominent reflection beneath the outer shelf might correspond to the base of the wedge (e.g., at 1.95 s TWT near CMP 10050, Figure 3b). Nearby, aggraded shelf sequences appear to be truncated by a steeply dipping unconformity (e.g., at 1.5 s TWT near CMP 9850, Figure 3b) which can be traced

northward, where it appears to merge with a discordant acoustic boundary beneath the continental slope.

[19] Northwest of CMP 9400 (Figure 3b), AWI-94003 crosses the continental slope and rise. Here, the slope is much shallower ($\leq 3^\circ$) than that observed to the northeast. Beneath the mid-lower slope, reflections appear to terminate downdip against an undulating acoustic boundary (e.g., at 4.8 s TWT near CMP 7020, Figure 3b), giving an impression of downlap. However, we do not interpret this boundary as a downlap unconformity, as this would imply deposition of most rise sediments (north of CMP 5600, Figure 3b) before the start of progradation of the adjacent continental slope. Instead, we interpret this feature as the migrating locus of an acoustic facies boundary corresponding to the base of the continental slope. Profiles BAS923-22, AWI-94040, and AWI-94042 show similar reflections (Figures 3c, 3d, and 3g described below). Northwest of c. CMP 7800, the top of oceanic basement is imaged at 6–8 s TWT (Figure 3b).

2.3.3. BAS923-22

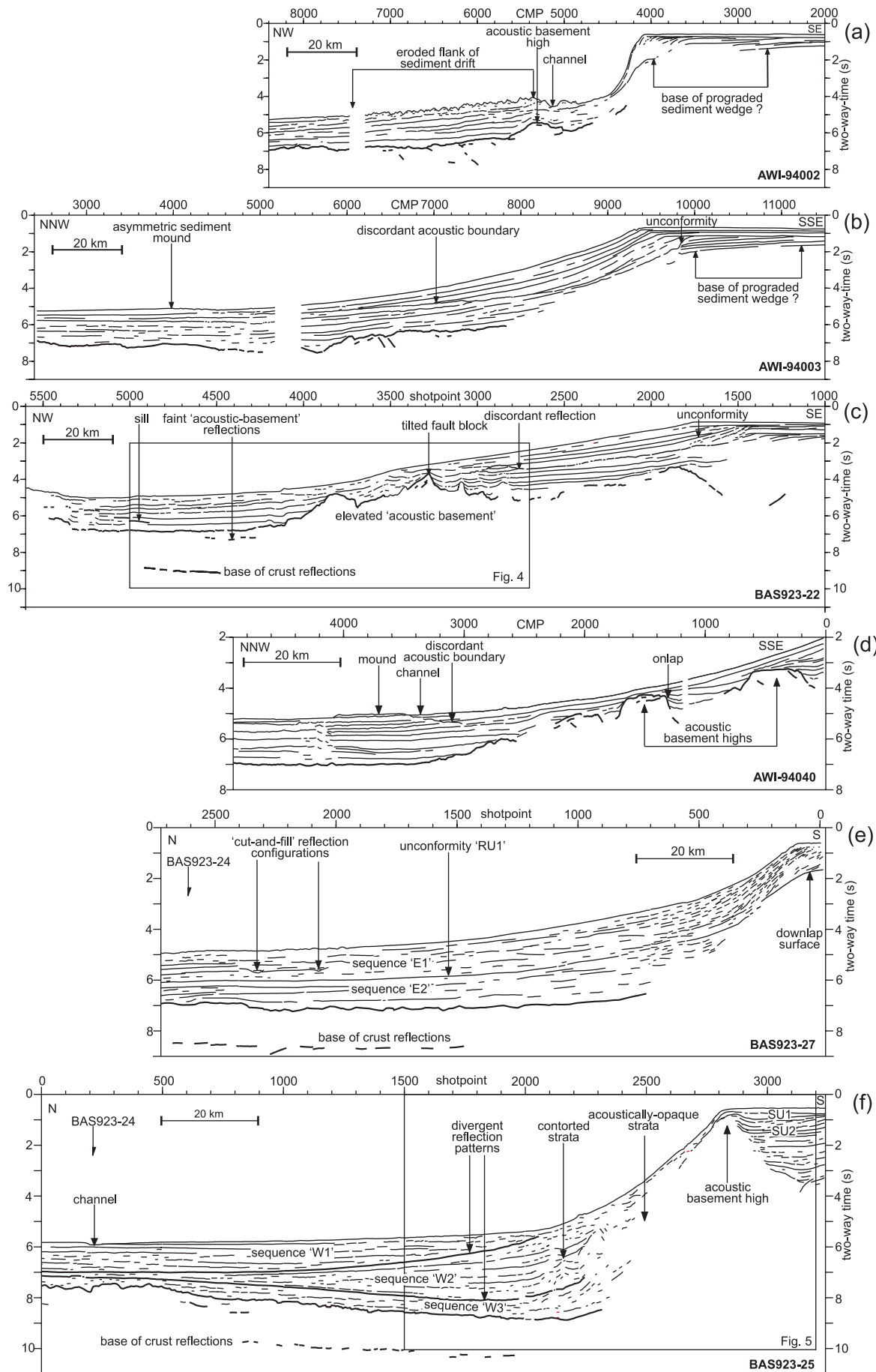
[20] Profile BAS923-22 (along 320°, Figures 2a and 3c, and 4) crosses the shelf edge and CSGA near 86°30'W. Magnetic data do not constrain oceanic basement age here (Figure 2b), although surrounding magnetic anomalies suggest that it is probably >44 Myr old [Larter *et al.*, 2002] (Figure 5).

[21] BAS923-22 shows faint acoustic basement beneath the shelf (e.g., at 4.0 s TWT near shot point SP 1700, Figure 3c), overlain by undulating reflections of presumed sedimentary origin (e.g., at 3.1 s TWT near SP 1700, Figure 3c). These strata are overlain in turn by a thick prograded sediment wedge [Nitsche *et al.*, 2000].

[22] North of SP1740, BAS923-22 crosses the continental slope (gradient $\leq 2.5^\circ$) and rise (Figure 3c). Here, the profile shows rugged acoustically opaque buried topography beneath the mid-lower slope, including a tilted fault block (near SP 3280, Figures 3c and 4). The buried topography coincides with the CSGA low (Figure 2a). Overlying sediments onlap the fault block (e.g., at 4.0 s TWT near SP 3260, Figures 3c and 4), and have draped and filled in the buried highs. Farther northwest, the reflection from the top of the acoustically opaque material merges with that defining the top of the neighboring oceanic basement.

[23] On the upper slope, we identify a slope-front sequence which unconformably overlies more steeply dipping shelf foresets (e.g., at 1.7 s TWT near SP 1740, Figure 3c), and which shows fairly continuous, regular reflections. This sequence probably consists mainly of mud and silt deposited by contour currents [Nitsche *et al.*, 2000].

[24] Farther northwest, BAS923-22 shows the very smooth top of oceanic basement southeast of Peter I Island. Here, the base of the crust is imaged clearly (e.g., at 9.1 s TWT near SP 4500, Figures 3c and 4). Very faint “intra-basement” reflections are visible beneath the base of slope (e.g., at 7.2 s TWT near SP 4300, Figures 3c and 4). Northwest of c. SP 5240, rise sediments show reduced reflection continuity (Figure 3c). This is probably a result of processes associated with Peter I Island, such as intrusion by dykes and sills, and deposition of debris flow deposits from the flanks of the volcano. Occasional, very high amplitude reflections are interpreted as sills (e.g., at 6.3 s TWT near SP 4940, Figures 3c and 4).



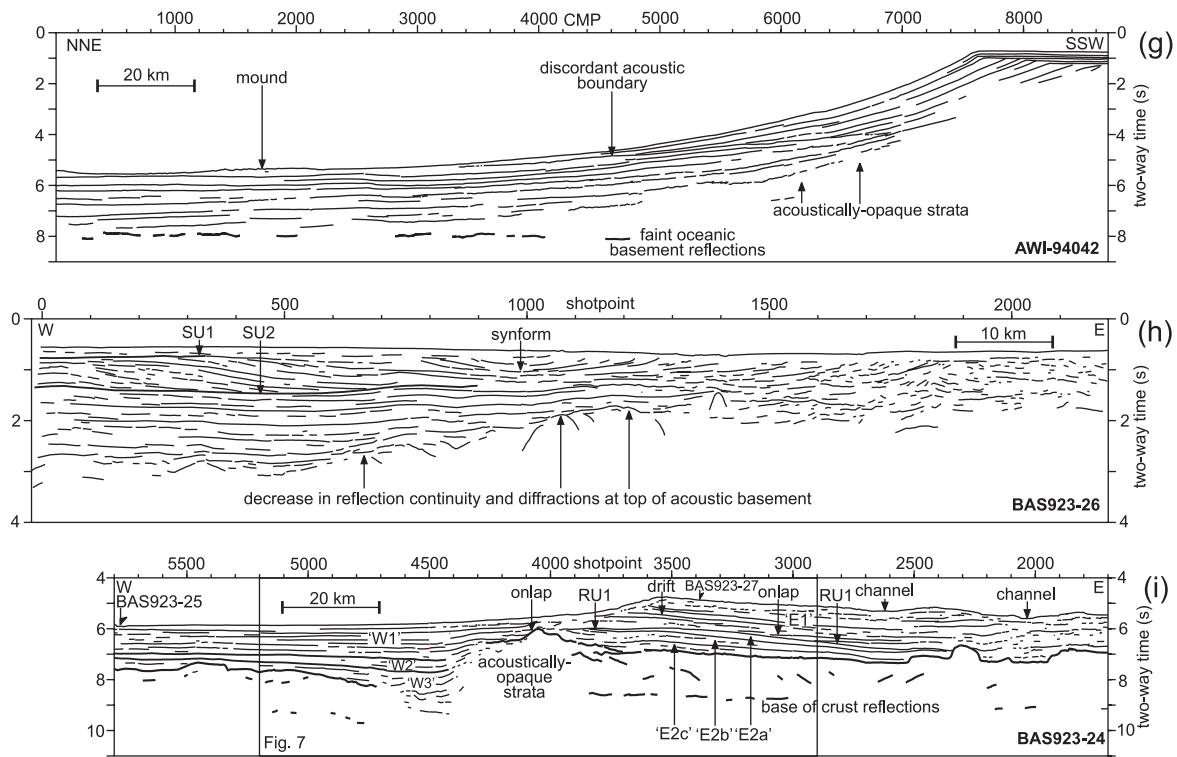


Figure 3. (continued)

2.3.4. AWI-94040

[25] Profile AWI-94040 (along 347° , Figures 2a and 3d) crosses the mid-lower slope and CSGA near 90°W . Magnetic data do not constrain oceanic basement age in this area (Figure 2b).

[26] South of CMP 3400, AWI-94040 shows acoustically opaque buried topography beneath the slope which coincides with the CSGA low (two highs near CMPs 400 and 1500, Figure 3d). Overlying sediments onlap the highs (e.g., at 4.7 s TWT near SP 1300, Figure 3d), and have filled in the buried topography. North of c. CMP 3450, the very smooth top of oceanic basement is imaged at 6.9–7.1 s TWT (Figure 3d). At shallower depth, the profile shows a channel-and-mound depositional system near CMP 3350 (Figure 3d). A discordant reflection dips southward from the northern edge of the channel. We interpret this as an acoustic facies boundary, which describes the northward migration of the channel.

2.3.5. BAS923-27

[27] Profile BAS923-27 (along 0° , Figures 2a and 3e) extends along the BGA high, and crosses the shelf edge near 94°W . Magnetic data do not constrain oceanic basement age in this area (Figure 2b).

[28] South of SP 90, BAS923-27 shows a prograded sediment wedge beneath the outer shelf [Nitsche *et al.*, 2000] (Figure 3e). The wedge is bounded beneath by a downlap unconformity (e.g., at 1.7 s TWT near SP 20,

Figure 3e) which we trace northward to c. SP 220 (at 2.8 s TWT, Figure 3e).

[29] North of SP 90, BAS923-27 crosses the continental slope (gradient $\leq 7^\circ$) and rise (Figure 3e). Here, the top of oceanic basement is very smooth (north of c. SP 700, at 6.5–7.3 s TWT, Figure 3e), and base-of-crust reflections (e.g., at 8.7 s TWT near SP 1500, Figure 3e) define a fairly uniform basement TWT thickness of c. 1.6 s. We have divided the overlying sediments into seismic sequences “E1” and “E2,” separated by unconformity “RU1” (Figure 3e). E2 shows fairly regular reflections, whereas shallower E1 strata show more varied reflection patterns including buried “cut-and-fill” configurations (e.g., at 5.7 s TWT near SP 2320, Figure 3e).

[30] On BAS923-27, RU1 is represented by a high amplitude, continuous concordant reflection. However, intersecting east-west profile BAS923-24 (Figure 3i, described below) shows that this surface is an unconformity. At its southern limit, RU1 is aligned with the downlap unconformity identified beneath the outer shelf, although poor reflection continuity prevents explicit correlation between these unconformities.

2.3.6. BAS923-25

[31] Profile BAS923-25 (along 180° , Figures 2a and 3f, and 5) crosses the shelf edge and the BGA low near 97°W . PAC-MBL/PAC-BEL magnetic anomalies 33r and 34 located over 260 km to the north (Figure 2b) suggest that

Figure 3. (opposite) Interpreted line drawings of MCS profiles in the Bellingshausen Sea (located in Figure 2a). Vertical exaggeration = c. 7:1 at the seafloor. (a) AWI-94002, (b) AWI-94003, (c) BAS923-22 (area shown in Figure 4 is outlined), (d) AWI-94040, (e) BAS923-27, (f) BAS923-25 (area shown in Figure 5 is outlined), (g) AWI-94042, (h) BAS923-26 (plotted twice as large as the other profiles), (i) BAS923-24 (area shown in Figure 7 is outlined).

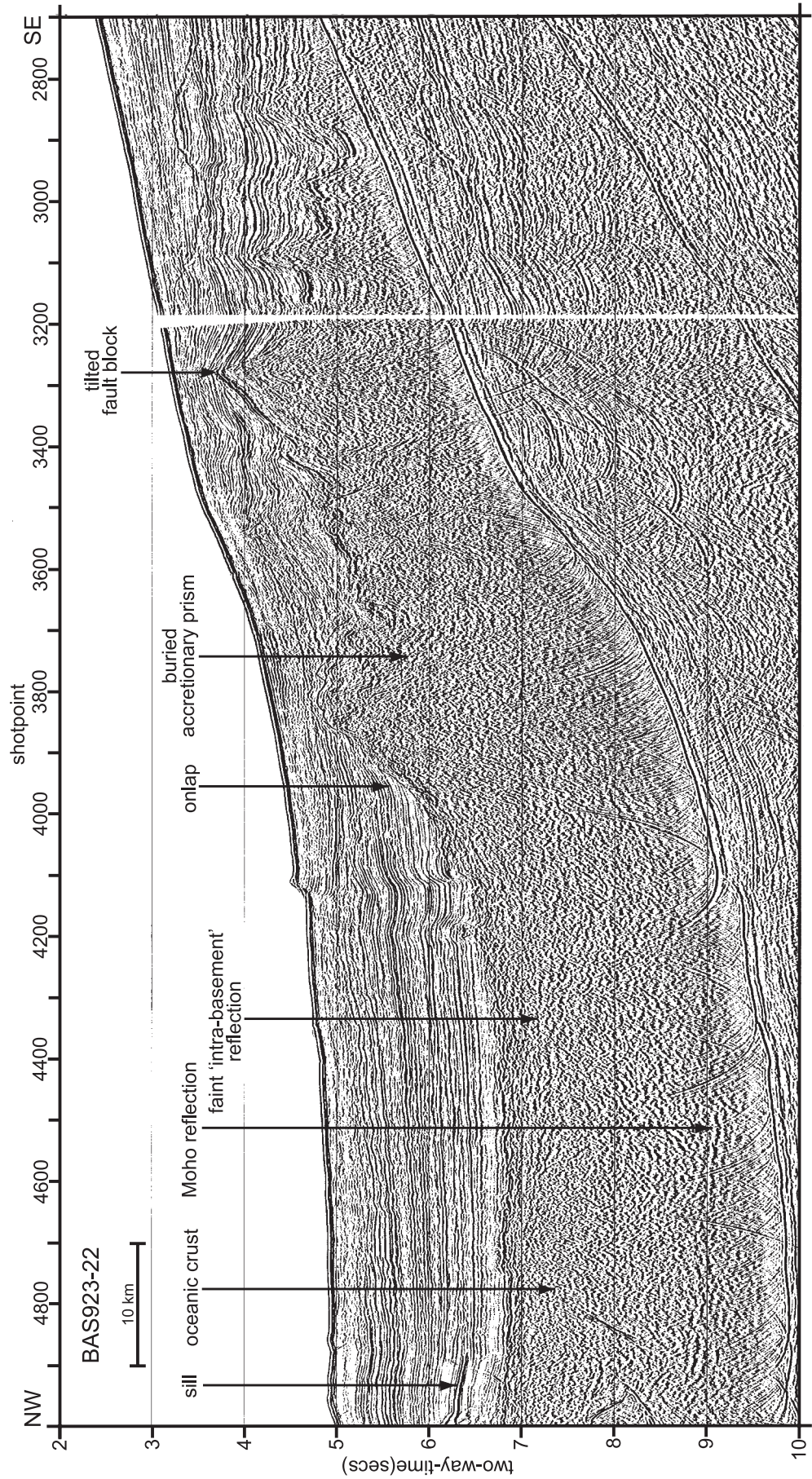


Figure 4. MCS profile BAS923-22 data panel (located in Figure 3c). These data were processed to 24-fold common-midpoint stack using standard procedures and time-migrated using a Stolt F-K algorithm. Vertical exaggeration = c. 8:1 at the seafloor.

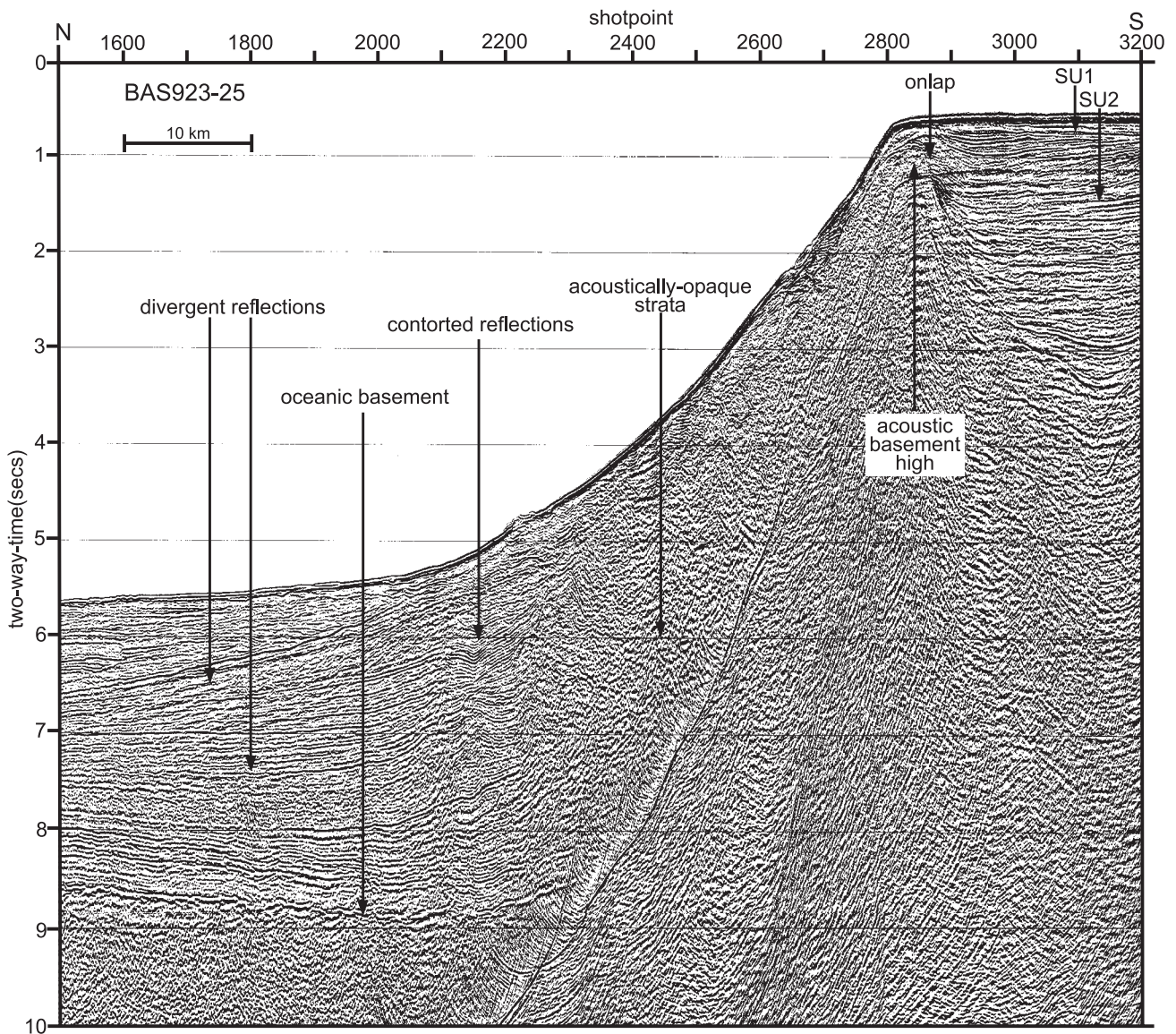


Figure 5. MCS profile BAS923-25 data panel (located in Figure 3f). These data were processed to 24-fold common-midpoint stack using standard procedures and time-migrated using a Stolt F-K algorithm. Vertical exaggeration = c. 8:1 at the seafloor.

oceanic basement imaged on this profile formed to the east of Chatham Rise at a precursor of the PAC-MBL/PAC-BEL ridge during the CNS, before breakup [Larter *et al.*, 2002, Figure 8b].

[32] On BAS923-25, the seismic architecture of the outer shelf differs greatly from that observed on neighboring profiles. Here, BAS923-25 shows a thick sedimentary succession landward of an acoustic-basement high which rises to 0.8 s TWT at the shelf edge. Older shelf sediments onlap the high (e.g., at 1.0 s TWT near SP 2875, Figures 3f and 5), whereas younger strata extend across it onto the slope. We identify two unconformities beneath the shelf (“SU1” and “SU2,” Figures 3f and 5) from intersecting east-west profile BAS923-26 (Figures 3h and 6 described below).

[33] Farther north, BAS923-25 crosses the steep continental slope (gradient $\leq 9^\circ$) and rise, and shows southward

dipping oceanic basement. Base-of-crust reflections indicate a southward reduction in basement TWT thickness from c. 1.65 s (at SP 850, Figure 3f) to c. 1.47 s (at SP 1950, Figure 3f). We have divided overlying sediments into seismic units “W1”, “W2”, and “W3” (Figure 3f). Unit W3 onlaps basement, has a fairly uniform TWT thickness south of SP 500, and a southerly component of dip which parallels that of underlying basement. W3 is conformably overlain by unit W2 which shows divergent reflections (e.g., between 6.5 and 8.0 s TWT near SP 1800, Figures 3f and 5) and a >13-fold increase in TWT thickness toward the margin. Although the geometry of W2 may partly reflect the continental sediment source to the south, its internal structure and dramatic northward thinning suggest to us that W2 deposition accompanied the southward tilting of basement. W3 and W2 strata become progressively contorted to the

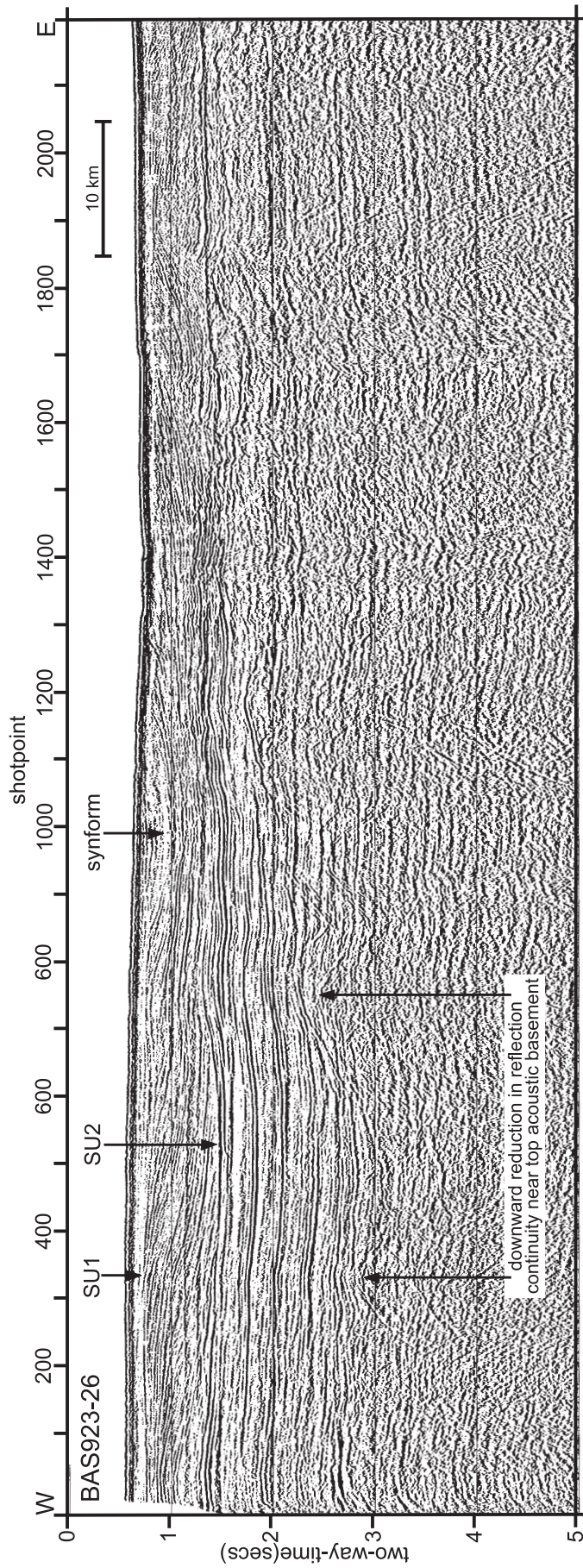


Figure 6. MCS profile BAS923-26 data panel (located in Figure 2a, and corresponding to Figure 3h). These unmigrated data were processed to 24-fold common-midpoint stack using standard procedures. Vertical exaggeration = c. 8:1 at the seafloor.

south, passing laterally into deformed, opaque acoustic facies beneath the lower slope (Figures 3f and 5). W1 thins toward the margin, and appears to onlap the top of W2, although the intervening boundary is poorly imaged. W1 strata show no signs of tectonic deformation.

2.3.7. AWI-94042

[34] Profile AWI-94042 (along 198°, Figures 2a and 3g) crosses the shelf edge near 104°30'W. The oceanic basement imaged on this line formed at the PAC-MBL ridge during the latter part of the CNS (Figure 2b), shortly after the separation of Chatham Rise from Marie Byrd Land.

[35] Southwest of CMP 7620 (Figure 3g), AWI-94042 shows a prograded sediment wedge beneath the outer shelf [Nitsche *et al.*, 1997, 2000]. Farther northeast, the profile crosses the continental slope (gradient $\leq 4^\circ$) and rise, where prograded shelf units extend northward to form a thick slope apron. Beneath the mid-lower slope, foreset reflections appear to terminate against an undulating discordant reflection (e.g., at 4.8 s TWT near CMP 4800, Figure 3g), which we interpret as the migrating locus of an acoustic facies boundary. At greater depth, AWI-94042 shows an opaque acoustic unit beneath the acoustically stratified slope sediments. Farther north, the faint top of oceanic basement is imaged at 7.7–8.3 s TWT (Figure 3g).

2.3.8. BAS923-26

[36] Profile BAS923-26 (Figures 2a and 3h, and 6) crosses the outer shelf and the continental part of the BGA off Thurston Island. The profile was shot along 084°, with minor course changes to avoid ice. Although BAS923-26 contains high-amplitude seafloor and peg-leg multiple reflections, some primary reflections can be traced to c. 3.0 s TWT.

[37] The western part of BAS923-26 shows the sedimentary succession imaged on BAS923-25 (landward of the basement high, Figures 3f and 5). The profile shows two shelf unconformities: “SU1” (e.g., at 0.75 s TWT near SP 320, Figures 3h and 6) and “SU2” (e.g., at 1.5 s TWT near SP 460, Figures 3h and 6). A synformal reflection pattern near SP 1000 (Figures 3h and 6) probably reflects a change in the depositional strike of prograded foresets relative to the trend of the profile. On this east-west line, the very faint top of acoustic basement is represented by a broad downward reduction in reflection continuity, accompanied by sparse diffractions (Figures 3h and 6).

2.3.9. BAS923-24

[38] Profile BAS923-24 (along 272°, Figures 2a and 3i, and 7) crosses the BGA near 69°30'S. We identify PAC-MBL/PAC-BEL anomalies 33r and 34 (Figure 2b) northwest of the BGA [Larter *et al.*, 2002]. Since seismic and gravity data show no evidence of crustal discontinuities between the BGA and these anomalies, we assume that all crust west of the BGA low (corresponding to c. SP 4250, Figure 3i and 7) formed at a precursor of the PAC-MBL/PAC-BEL ridge during the CNS. However, magnetic data do not constrain the age of the oceanic basement farther east on the profile (green ornament, Figure 2b). BAS923-24 crosses BAS923-25 (Figures 3f and 5) at SP 5776 and BAS923-27 (Figure 3e) at SP 3380.

[39] BAS923-24 shows that the BGA low corresponds to a buried asymmetric basement trough, formed where presumed CNS-age oceanic basement dips beneath more elevated basement to the east. Sediments within the base-

ment trough pass eastward into acoustically opaque material (east of c. SP 4400, Figures 3i and 7) which coincides with the BGA minimum [Gohl *et al.*, 1997a]. The profile also shows deformation increasing to the east within the trough, where sedimentary strata have been tectonically shortened and uplifted. The BGA maximum (centered on SP 3550, Figures 3i and 7), coincides with the elevated seafloor and basement east of the buried trough. Sediments within the trough have been divided into acoustic units W1, W2 and W3 (Figure 3i) on the basis of their geometry on intersecting profile BAS923-25 (Figure 3f). Sediments deposited farther east have been divided into separate sequences E1 and E2a–c (Figure 3i), because existing data do not permit correlation of these sequences with those in the trough.

[40] The oldest preserved W3 sediments onlap basement, and show that the western flank of the trough tilted eastward before they were deposited. Thus, profiles BAS923-25 and BAS923-24 (Figures 3f and 3i) together describe two separate phases of deformation; basement forming the western trough flank was initially tilted to the east, which was followed by the deposition of W3 sediments. Subsequently, W2 deposition accompanied the tilting of basement toward the south. BAS923-24 suggests that W3 strata were horizontally layered when deposited, and were later deformed and uplifted. The eastern part of unit W2 has been deformed in a similar way. However, tectonism ceased with, or shortly after, the onset of W1 deposition. Younger W1 strata onlap the acoustically opaque unit (e.g., at 6.1 s TWT near SP 4080, Figures 3i and 7), and show no signs of deformation.

[41] East of the trough, we identify the two seismic sequences E1 and E2 (divided into subunits E2a, E2b and E2c, Figure 3i) separated by unconformity RU1 (Figures 3i and 7). The oldest subunits E2b and E2c thicken westward toward the trough, whereas subunit E2a thins toward the trough, west of c. SP 3240 (Figure 3i). Westward thinning of E2a results mainly from erosion, since E2a and E2b reflections are truncated beneath RU1 (e.g., at 6.0 s TWT near SP 3845, Figures 3i and 7). To the east, subhorizontal E1 strata onlap RU1 (e.g., at 6.3 s TWT near SP 3060, Figures 3i and 7). The proximity of RU1 to the basement trough and the eastward tilt of basement beneath it suggest to us that the unconformity has a tectonic origin. In particular, we infer that oceanic basement east of the trough was uplifted prior to the onset of E1 deposition, and that RU1 was once the flank of a bathymetric high. Oldest E1 strata have an east component of dip of $<0.5^\circ$ (assuming a sediment velocity of 1800 m.s^{-1} , between SPs 2560 and 2940, Figure 3i), which suggests that basement tectonism had diminished greatly, or ceased entirely, by the time of E1 deposition. The upper part of E1 shows a well-formed sediment drift, with deep-sea channels and migrating sediment waves [Nitsche *et al.*, 2000].

2.4. Gravity Modeling

[42] We have produced simple models of the free-air gravity anomaly along profiles BAS923-22, BAS923-25 and BAS923-26, using MCS data to define the shallow structure, and hence to constrain deep structure (Figures 8, 9, and 10). To illustrate the range of possible basement structures which ambiguities in the models permit, we present two models for each profile: one showing a hypothetical basement configuration in areas where depths to the

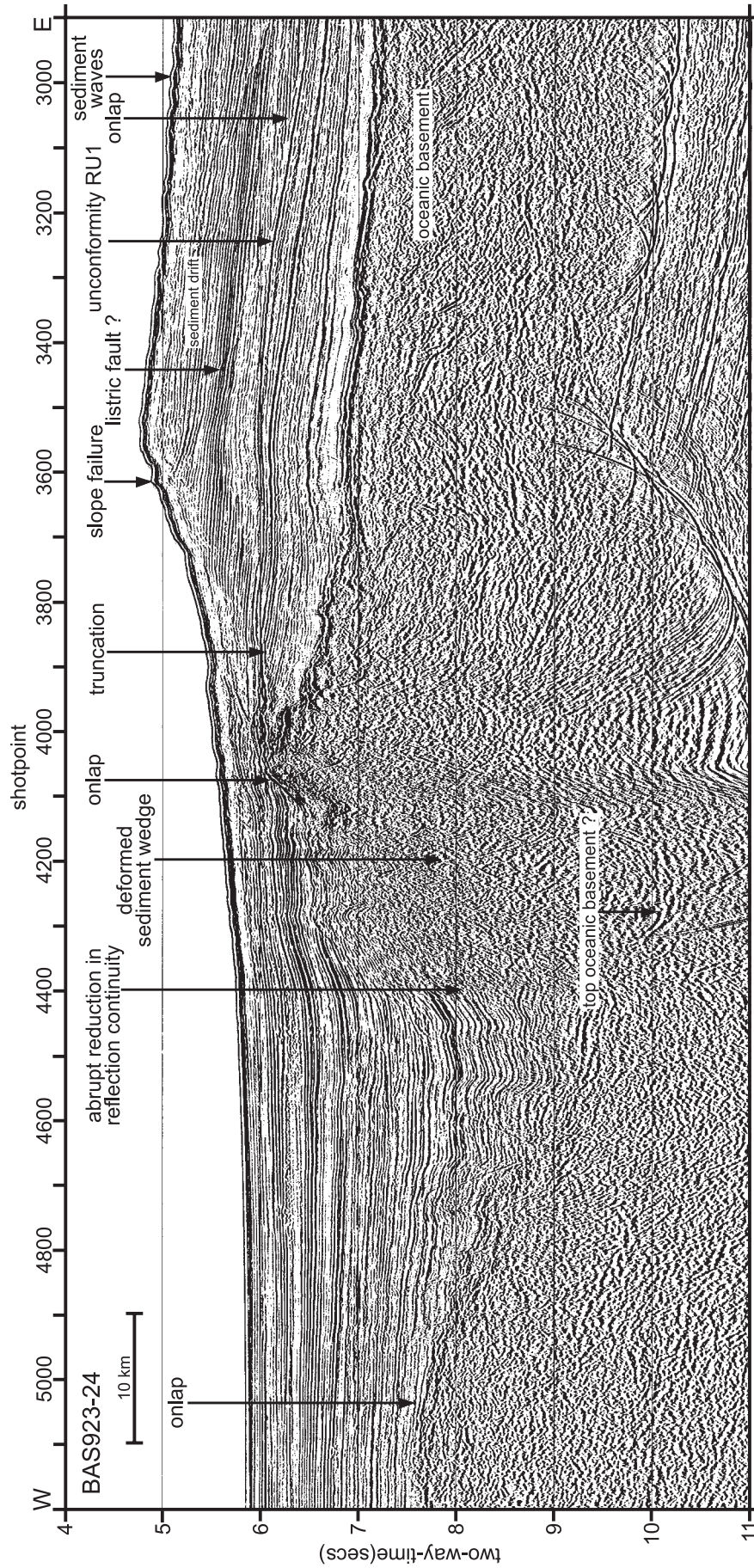


Figure 7. MCS profile BAS923-24 data panel (located in Figure 3i). These data were processed to 24-fold common-midpoint stack using standard procedures and time-migrated using a Stolt F-K algorithm. Vertical exaggeration = c. 8:1 at the seafloor.

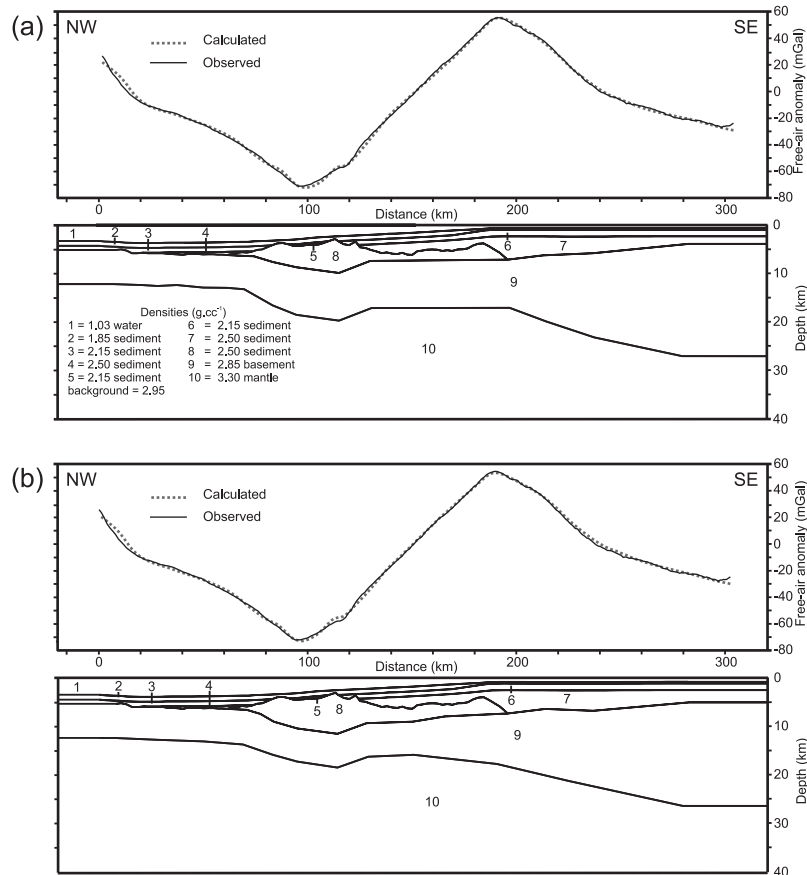


Figure 8. Models of free-air gravity anomaly along MCS profile BAS923-22 (located in Figure 2a). The observed gravity data were projected from their true positions onto a track along 320° before modeling, to ensure that the data were correctly positioned in the model plane of section. (a) shows a hypothetical basement configuration with body 8 (interpreted as a buried accretionary prism) of minimum practicable thickness, and (b) shows our preferred interpretation.

top of basement are poorly constrained, and the other showing our preferred interpretation. JR04 gravity data have been reduced using standard procedures.

2.4.1. BAS923-22 Gravity Model

[43] Figure 8 shows the free-air gravity anomaly along profile BAS923-22. The CSGA low is centered on 97 km along-track. In the absence of deep seismic velocity information, we used velocity-depth [Hamilton, 1979] and velocity-density [Ludwig *et al.*, 1970] relationships to estimate the density structure of undeformed slope and rise sediments. Hamilton [1979] proposed the following empirical equation for deep-water clastic turbidite sediments:

$$V = 1.511 + 1.304D - 0.741D^2 + 0.257D^3 \quad (1)$$

where V is compressional-wave velocity, km s^{-1} and D is depth below seafloor, km. Equation 1 predicts velocities of 1.51, 2.33, and 3.21 km s^{-1} at the seafloor and subbottom depths (SBDs) of 1 and 2 km, respectively. On these grounds, we assume a gross velocity structure of 1.92 km s^{-1} for 0–1 km SBD, and 2.77 km s^{-1} for 1–2 km SBD for undeformed rise sediments (with corresponding densities of 1.85 and 2.15 g cc^{-1} [Ludwig *et al.*, 1970], bodies 2, 3, 5 and 6 (Figure 8)). Undeformed sediments below 2 km SBD (included in bodies 4 and 7) have been assigned a density of

2.50 g cc^{-1} (equivalent velocity of 4.45 km s^{-1}), which we propose for more deeply buried and consolidated clastic sediments. For consistency, we calculated the depth to the top of “acoustic basement” using the same velocities.

[44] Farther south, we used semblance analyses to estimate the shallow velocity structure of the continental shelf because: (1) anomalous sediment velocities have been reported elsewhere beneath the West Antarctic shelf [Larter and Barker, 1989; Cochrane and Cooper, 1992]; and (2) this part of the profile shows numerous near-horizontal primary reflections, and so semblance analyses should yield reliable interval velocities at shallow depth. Twenty eight semblance analyses suggest a gross velocity structure of 2.37 km s^{-1} for 0–1 km SBD, and 3.08 km s^{-1} for 1–2 km SBD. Ludwig *et al.* [1970] predict corresponding densities of 2.05 and 2.25 g cc^{-1} , but in practice, we have adjusted the boundaries of bodies 2 and 6 continued from deeper water to provide an equivalent mass between 0 and 2 km SBD. A section of “acoustic basement” thought to be composed of deformed sediment (body 8) has been assigned a density of 2.50 g cc^{-1} . An important initial assumption is that basement beneath the base of slope (at 50 km along-track, Figure 8) has a typical oceanic thickness of 7 km [e.g., White *et al.*, 1992]. Here, the MCS data show an oceanic basement TWT thickness of c. 2 s, consistent with

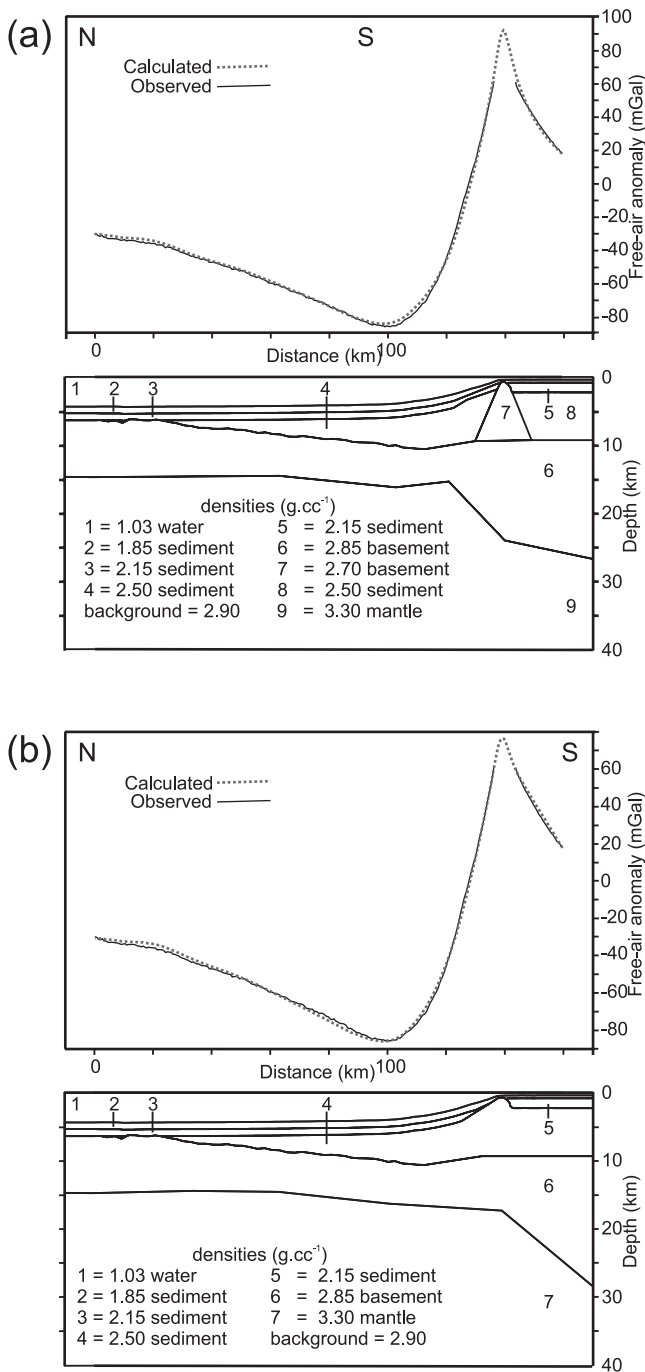


Figure 9. Models of free-air gravity anomaly along MCS profile BAS923-25 (located in Figure 2a). The observed gravity data were projected from their true positions onto a track along 180° before modeling, to ensure that the data points were correctly positioned in the model plane of section. (a) shows a hypothetical basement configuration which includes body 7 with an upper crustal basement density beneath the shelf edge, and (b) shows our preferred interpretation. There is a gap in the observed profile from 136–144 km along track.

this assumption. In most models, basement crust and mantle have been assigned uniform densities of 2.85 and 3.30 g cc⁻¹, respectively (bodies 9 and 10, Figure 8).

[45] There are several sources of uncertainty in our gravity models. Our estimates of the density of undeformed sediments could be affected by an unexpected burial history, or from errors in semblance velocity picks. Also, we expect that our initial assumption of basement thickness will result in a systematic error in basement thickness on each profile. Furthermore, the following parameters remain poorly constrained:

1. The density of sediments below 2 km SBD and deformed sediments forming shallow “acoustic basement” (set to 2.50 g cc⁻¹). This parameter could range between 2.23 g cc⁻¹ (sediment density at 2 km SBD implied by Hamilton [1979] and Ludwig *et al.* [1970]) and about 2.7 g cc⁻¹ (the maximum for consolidated clastic sediments).

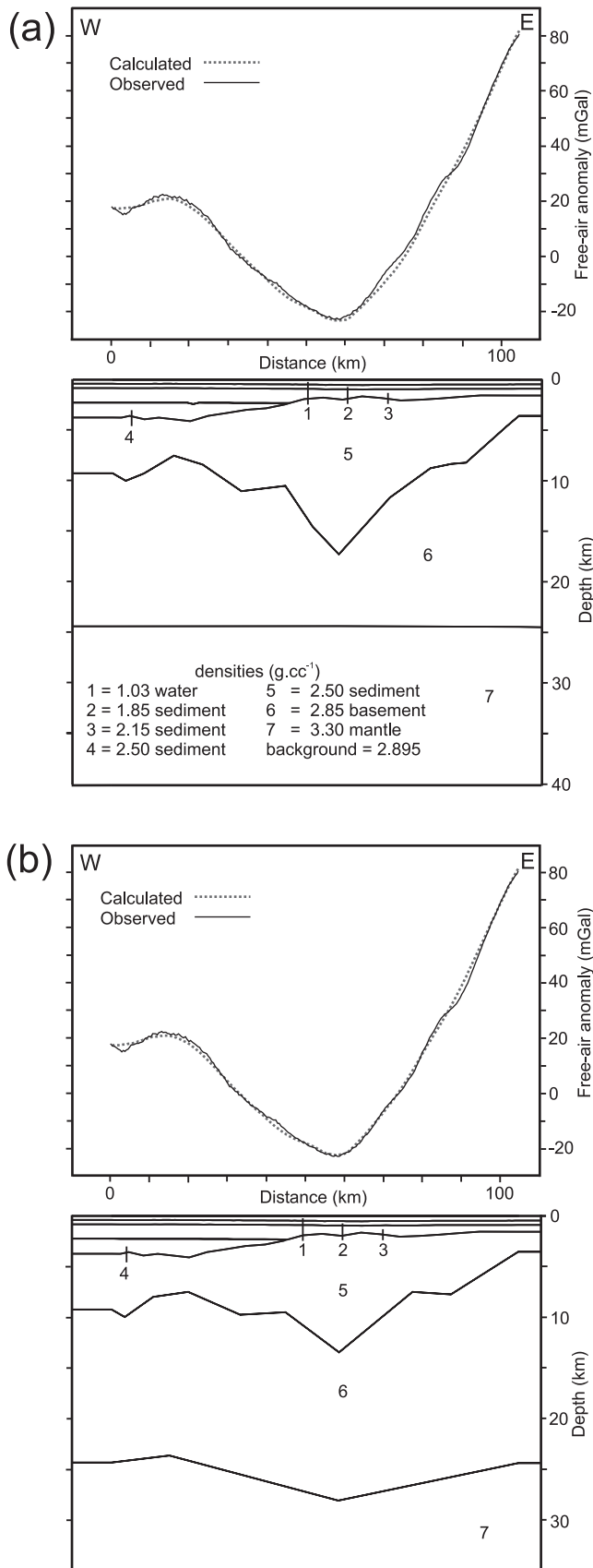
2. The depth to the top of basement in areas where it is not clearly imaged on MCS profiles. In this study, we present alternative models to illustrate the trade-off between the thicknesses of intermediate density material and basement in such areas.

3. The density of basement crust (set to 2.85 g cc⁻¹ in our preferred models). Mean oceanic and continental crustal densities are 2.89 [Carlson and Raskin, 1984] and 2.835 g cc⁻¹ [Christensen and Mooney, 1995], respectively. Hence, we anticipate comparatively small errors between the assumed and actual mean basement crust densities.

[46] We present two models of the free-air gravity along BAS923-22: one showing a hypothetical basement configuration beneath the CSGA low (Figure 8a), and the other showing our preferred interpretation (Figure 8b). The CSGA low is most easily reconciled with comparatively low density (2.50 g cc⁻¹) “acoustic basement” topography beneath the lower slope, which forms a northward tapering wedge north of the anomaly minimum (body 8, Figure 8). Figure 8a shows that the observed data can be matched with 10 km-thick basement beneath the CSGA. In this model, the top of crystalline basement (body 9) rises close to the inferred depth of “acoustic basement” imaged beneath the upper slope (top of body 8, near 150 km along track). This suggests that 10 km basement thickness is close to the maximum possible at this point (estimated from other models to be c. 11.5 km), since crystalline basement cannot extend above “acoustic basement” in the MCS data. In our preferred interpretation (Figure 8b), we model the observed gravity using 7 km thick basement crust beneath the CSGA low. In practice, we can match the observed data using even thinner crust, although these interpretations become increasingly unrealistic. Therefore, our models show that the CSGA low can be reconciled with a body of density 2.5 g cc⁻¹ beneath the buried topography, underlain by intermediate or oceanic thickness basement.

2.4.2. BAS923-25 Gravity Model

[47] Figure 9 shows the free-air gravity anomaly along profile BAS923-25. The BGA low is centered on 100 km along-track. Undeformed slope and rise sediments are again assigned densities of 1.85, 2.15, and 2.50 g cc⁻¹, for 0–1, 1–2, and >2 km SBD, respectively (bodies 2, 3, 4, 5 and 8, Figure 9). Eight semblance analyses suggest a gross velocity structure beneath the outer shelf of 2.23 km s⁻¹ for 0–1 km SBD, and 2.93 km s⁻¹ for 1–2 km SBD. Ludwig *et al.*



[1970] predict corresponding densities of 2.02 and 2.20 g cc^{-1} , and we have adjusted bodies 2 and 5 to provide an equivalent mass between 0 and 2 km SBD. An important initial assumption is that the basement at 40 km along-track has a typical oceanic thickness of 7 km. The MCS profile shows oceanic basement TWT thicknesses of 1.47–1.65 s. This range is less than that of typical oceanic basement, suggesting that it might actually be thinner than normal. If so, actual basement thicknesses will be systematically smaller than indicated in the models.

[48] Figure 9a shows a hypothetical basement configuration beneath the outer shelf, and Figure 9b shows our preferred interpretation. The “acoustic basement” high imaged in the MCS data could be composed of continental basement material. To test this, we substituted the high with a triangular body (body 7, Figure 9a) with a typical upper continental basement density of 2.7 g cc^{-1} (maximum basement thickness = c. 23 km). In this model, we fit the observed data by adjusting the underlying base of crust (body 6/9 interface).

[49] In our preferred interpretation (Figure 9b), the “acoustic basement” high is composed of deformed sediment (body 4, set to 2.50 g cc^{-1}), underlain by 8 km thick crystalline basement. In practice, we can match the observed data using even thinner basement beneath the high, although these interpretations become increasingly unrealistic. Hence, on the basis of these two models, we cannot distinguish whether the “acoustic basement” high is composed of deformed sediment or continental basement crust. Farther north, the BGA low is explained by a northward-tapering sediment wedge beneath the upper slope, which attains a thickness of c. 8.2 km in our preferred model (near 133 km along-track, Figure 9b). The gentle curvature of the observed anomaly north of the gravity minimum has been modeled by thickening the oceanic basement northward (from <6 km to c. 8.2 km thick at the northern end of line, Figures 9a and 9b). This is consistent with the northward increase in basement TWT thickness in the MCS data (Figure 3f). Alternatively, this trend could be due to a southward increase in the seismic velocity (and density) of oceanic layer 2 resulting from consolidation as its depth of burial increases.

2.4.3. BAS923-26 Gravity Model

[50] Figure 10 shows the free-air gravity anomaly along profile BAS923-26. The continental part of the BGA low is centered on 58 km along-track. Seventeen semblance analyses suggest a gross velocity structure for sediments beneath the outer shelf of 2.22 km s^{-1} for 0–1 km SBD, and 2.88 km s^{-1} for 1–2 km SBD. This closely resembles the velocity structure at the southern end of line BAS923-25, and we have tied the structure of the two gravity models where they intersect. Hence, we have assumed 15 km thick

Figure 10. (opposite) Models of free-air gravity anomaly along MCS profile BAS923-26 (located in Figure 2a). The observed gravity data were projected from their true positions onto a track along 83° before modeling, to ensure that the data points were correctly positioned in the model plane of section. (a) shows a hypothetical basement configuration with no Moho topography, and (b) shows our preferred interpretation.

basement at the western end of the line. At the western end of the model, we have also added an additional boundary representing the top of the very faint “acoustic basement” imaged in the MCS data (body 4/5 interface). However, this does not affect the tie with the BAS923-25 model, as the top of body 5 has a zero density contrast on this part of the profile.

[51] In Figures 10a and 10b, undeformed sediments below 2 km SBD (body 4) and “acoustic basement” (body 5) have been set to 2.50 g cc^{-1} . For this profile, we have assumed that the model bodies have infinite strike length. However, Figure 9 shows that the base of the crust probably dips across the plane of section, and that some shallow bodies have quite limited strike extent.

[52] Figure 10a shows a hypothetical basement configuration beneath the outer shelf, and Figure 10b shows our preferred interpretation. Figure 10a shows that the continental BGA low can be reconciled with thick sediments underlain by 7 km thickness basement (keeping the base of crust fixed at 24 km depth), although we doubt the existence of such thin basement beneath this part of the shelf. Alternatively, the faint “acoustic basement” imaged beneath the shelf could be composed of continental basement material (as considered for BAS923-25, Figure 9a), and to test this, we generated additional models with body 5 set to 2.7 g cc^{-1} . However, after substituting the thick sedimentary section with continental basement, we had to include extreme topography on the base of the crust to match the observed anomaly. Also, the much reduced density contrast at the body 5/6 boundary meant that we could not easily match the shorter wavelength components of the anomaly. In our preferred interpretation (Figure 10b), we have modeled the continental BGA low with thick consolidated sediments, and a slightly greater depth to the base of the crust beneath this part of the shelf. In this model, the important density contrast is generated at the body 5/6 interface, which is below the top of “acoustic basement” identified on the seismic profile. Hence, the sedimentary units observed in the seismic data cannot account for the BGA low, which must therefore result from lateral variation at greater (mid crustal) depth. The model also suggests a marked difference in the thickness of the crystalline basement beneath the western and eastern ends of the profile (15 km in the west, and 21 km in the east, Figure 10b).

3. Discussion

[53] Marine geophysical data presented in this study describe tectonic structure, and provide new insights into the geological development of the West Antarctic continental margin. Here, we consider the origin of the tectonic structures which generate the CSGA and the BGA in the light of our new tectonic framework [Larter *et al.*, 2002].

3.1. Origin of the Continental Slope Gravity Anomaly (CSGA)

[54] MCS profiles BAS923-22 and AWI-94040 (Figures 3c, 3d, and 4) show that the CSGA coincides with acoustically opaque topography buried beneath the mid-lower slope. The buried topographic highs are dissected by extensional faults, and one prominent peak has the appearance of a tilted fault block.

[55] Although BAS923-22 (Figures 3c and 4) images buried topography, these near-normal-incidence data do not define its nature or composition. However, accompanying gravity models provide additional constraint (Figure 8), and show that the observed anomaly can be modeled by assigning this material a density of 2.50 g cc^{-1} . This density falls within the range for consolidated sedimentary rocks [Ludwig *et al.*, 1970; Dobrin, 1976], which suggests that the buried topographic highs are probably composed of deformed and consolidated sediment. Our preferred model (Figure 8b) shows oceanic basement dipping southward beneath the sediment wedge. It is unclear why the MCS profile fails to show a clear contact between deformed sediment and crystalline basement, although consolidation of the deepest sediments may have reduced the acoustic impedance contrast at this boundary.

[56] On the basis of our new reconstructions [Larter *et al.*, 2002], we suggest that the buried topography represents the top part of an accretionary prism which formed during southward subduction of the Phoenix plate, and the subduction of at least one plate fragment derived from it. Magnetic anomalies and gravity lineations in the western Pacific [Larter *et al.*, 2002, Figure 3] show that the westernmost part of the Phoenix plate broke off the main part of that plate during the CNS, and we refer to this fragment as the “Charcot” (CHA) plate. The reconstructions suggest also that the Charcot plate was subducted at this part of the Antarctic Peninsula margin during the CNS. Although the MCS data show extensional deformation within the sediment wedge, we still infer that this body formed initially in a convergent tectonic setting: the extension could have occurred in a forearc setting (as reported in modern forearcs by Aubouin *et al.* [1984], Bourgois *et al.* [1988], and Vanneste and Larter [2002]), or it could have occurred after the cessation of convergence.

[57] Farther east and west, the CSGA suggests continuity of the buried accretionary prism (from 83 to 93°W , Figure 2b). At its western limit, the CSGA is intersected by the north-south trending BGA high. Farther east, the anomaly decreases sharply in amplitude near 87°W , before it finally fades near 83°W , close to the southwestern limit of ocean floor known to have formed at the ANT-PHO ridge (Figure 2b). MCS profiles crossing the margin northeast of the CSGA show no evidence of an extensive buried accretionary prism [Larter and Barker, 1991b].

[58] Although our results suggest the existence of a buried accretionary prism, we cannot determine its age precisely on the basis of available data. Magnetic profiles in the area surrounding Peter I Island do not define a clear pattern of lineations, and so the age of the oceanic basement extending beneath the accretionary prism remains uncertain. Our new reconstructions [Larter *et al.*, 2002] suggest that this ocean floor probably formed on the Charcot plate during the CNS, and that Charcot plate subduction probably ceased before chron 34 (83 Ma). After the cessation of subduction, the surviving fragment of the Charcot plate became coupled to the Antarctic Peninsula across the stalled subduction zone. On these grounds, we infer that the development of the accretionary prism probably ceased during the CNS.

3.2. Tectonic Style of the Margin and Slope Morphology

[59] Although magnetic anomalies [*Herron and Tucholke, 1976; Barker, 1982; Larter and Barker, 1991a*] show that Phoenix plate subduction occurred at the Antarctic Peninsula margin northeast of the CSGA, MCS profiles show no evidence of an extensive buried accretionary prism beneath this part of the margin [*Larter and Barker, 1991b*]. Furthermore, there is an abrupt change in the overall gradient of the continental slope at about 78°W, which is well illustrated by profiles AWI-94002 and AWI-94003 (Figures 3a and 3b). On profiles crossing the Bellingshausen Sea continental margin between 94°W and 78°W, the continental slope has a gentle gradient ($\leq 7^\circ$), but all profiles crossing the Antarctic Peninsula continental margin between 78°W and 64°W show midslope (1000–2000 m depth) gradients exceeding 10° [*Larter et al., 1997*]. The gradient of the continental slope at the Antarctic Peninsula Pacific margin has certainly increased during the Pliocene and Pleistocene as a result of progradation [*Larter and Cunningham, 1993; Larter et al., 1997*], but where the base of the prograding/aggrading sequences has been imaged, a steep lower paleoslope is generally revealed, as on profile AWI-94002 (Figure 3a). The reasons for these changes in the tectonic style of the margin remain uncertain. However, our new tectonic framework [*Larter et al., 2002*] suggests to us that the topography of the subducted Phoenix plate may have been an important factor. *McCarron and Larter* [1998] reported a dramatic decrease in the rate of ANT-PHO spreading at chron 23r (52.3 Ma) from half rates of 51 to 21 mm.yr⁻¹, which was probably accompanied by an increase in the roughness of the abyssal hill fabric generated at the ridge (e.g., *Bird and Pockalny* [1994]). Therefore, the part of the margin where Phoenix plate subduction continued after chron 23r (in effect, all parts bordered by recognizable Tertiary magnetic anomalies) may have been subjected to subduction erosion associated with the subduction of rough basement topography [e.g., *Lallemant and Le Pichon, 1987; Ballance et al., 1989; von Huene and Scholl, 1991*]. The extent of subduction erosion may be expected to increase northeastward across each FZ, as subduction of rough ANT-PHO ocean floor continued for increasing lengths of time northeastward along the margin. Furthermore, reconstructions suggest that the onset of ANT-PHO spreading at the DGGa at chron 27 (61 Ma) resulted from a westward ridge jump from a former BEL-PHO spreading center [*Larter et al., 1999*]. We infer that subduction of the abandoned BEL-PHO ridge topography may have also contributed to subduction erosion of the margin. Hence, subduction erosion of the Antarctic Peninsula margin may explain why we find no evidence of an extensive buried accretionary prism east of 83°W, and partly explain why the Antarctic Peninsula continental slope is consistently steeper than that observed in the Bellingshausen Sea to the southwest.

3.3. Origin of the Bellingshausen Gravity Anomaly (BGA)

[60] MCS profiles crossing the BGA low on the continental rise (BAS923-24, Figures 3i and 7, and AWI-94041 of *Gohl et al.* [1997a]) show that it corresponds to a buried asymmetric basement trough, where presumed CNS-age

(83–118 Ma) oceanic basement dips beneath more elevated oceanic basement to the east. MCS and gravity data also show that tectonic convergence within the trough has resulted in the development of a thick, deformed sediment wedge which coincides with the gravity minimum [*Gohl et al., 1997a*]. Farther south, profile BAS923-25 (Figures 3f and 5) shows that the basement beneath the western flank of the trough also dips southward beneath the West Antarctic margin, where the BGA low extends onto the continental shelf (near 95°30'W). *McAdoo and Laxon* [1997] suggested that the BGA low continues across the West Antarctic margin as the western branch of their “De Gerlache-Peter I Island lineation.” The free-air gravity anomaly profile along BAS923-26 supports this view. Our models for this gravity anomaly show that the continental part of the BGA low can be modeled by thick consolidated sediments, possibly combined with a slightly greater depth to the base of the crust beneath this part of the shelf (Figure 10).

[61] Previous studies provide conflicting explanations for the origin of the BGA: *Gohl et al.* [1997a] interpreted the BGA trough as a site of early Tertiary transpressional relative motion between the Bellingshausen and Phoenix plates, whereas *McAdoo and Laxon* [1997] attributed the BGA to Tertiary intraplate deformation. Although the asymmetric basement profile of the trough (on BAS923-24, Figures 3i and 7) resembles that of long-offset oceanic FZs, we do not interpret the trough as a typical fossil transform fault because (1) it is not aligned with FZs describing either PAC-MBL/PAC-BEL or ANT-PHO relative motion [*Gohl et al., 1997a*]; (2) vertical basement relief described by gravity modeling [*Gohl et al., 1997a*] exceeds that observed even at long-offset FZs (e.g., Romanche FZ [*Bonatti et al., 1994*]); and (3) MCS profile BAS923-25 (Figure 3f) shows clearly that deformation of the continental margin off Thurston Island, including tectonism of slope sediments, contributed to its development. Furthermore, marine magnetic data (Figure 2b) show that the DGGa and BGA lie between areas of ocean floor formed by PAC-MBL/PAC-BEL and ANT-PHO spreading. Our new reconstructions [*Larter et al., 2002*] suggest that the undated ocean floor immediately east of the trough may be a remnant of the Charcot plate, formed by PAC-CHA spreading during the CNS. We suggest that this remnant became coupled to the Antarctic Peninsula as Charcot plate subduction stalled, and that the BGA trough developed at its western edge as a plate boundary which accommodated a small amount of convergence.

[62] The timing of the initial formation of the trough and the development of the sediment wedge is uncertain because our MCS profiles lack reliable age control. Nevertheless, our new tectonic framework provides some loose constraint [*Larter et al., 2002*]. The MCS profiles reveal two separate phases of tectonism; basement underlying the western trough flank was first tilted to the east, and then to the south (section 2.3.9). The first phase of tectonism occurred relatively soon after the formation of the presumed CNS-age crust to the west, since the oldest preserved trough sediments directly onlap east-dipping basement. Although the initial rate of sedimentation within the trough is unknown, we anticipate that the nearby young, rifted West Antarctic continental margin would have provided an abundant supply of terrigenous sediment during the Late Cretaceous. Our

reconstructions for the CNS suggest that the BGA trough may have formed initially along a PAC-CHA FZ conjugate to gravity lineament "Y" [Larter *et al.*, 2002, Figure 8b]. Thus, ocean floor adjacent to both flanks of the BGA trough probably formed by PAC-CHA spreading.

[63] Previous tectonic reconstructions show that a BEL-PHO (BEL-Aluk) plate boundary must have existed in the Bellingshausen Sea during the Late Cretaceous and early Tertiary [Mayes *et al.*, 1990], and the BGA trough has been interpreted as a site of early Tertiary BEL-PHO obliquely convergent motion [Gohl *et al.*, 1997a]. However, BEL-PHO motion in the region of the BGA prior to chron 27 (61 Ma) is now estimated to have been divergent [McCarron and Larter, 1998; Larter *et al.*, 2002]. Therefore, the BGA trough is unlikely to have accommodated east-west BEL-PHO tectonic convergence during the Late Cretaceous, and an alternative explanation is required to account for its development as a convergent or obliquely convergent tectonic boundary. Our reconstructions [Larter *et al.*, 2002] suggest that the crust immediately east of the trough may have formed on the Charcot plate, and that it subsequently became coupled to the Antarctic Peninsula, following cessation of Charcot plate subduction at the continental margin. A similar process appears to have occurred with the suturing of the northernmost part of the Rivera plate to North America [DeMets and Wilson, 1997]. If a crustal fragment became coupled to the Antarctic Peninsula in this way, deformation in the BGA trough could have accommodated relative motion between the Antarctic Peninsula and another plate or plates to the west.

[64] In the absence of reliable timing constraints, the age of the BGA trough remains uncertain. However, W3 sediments onlap the dipping western flank of the trough, which suggests that it formed comparatively soon after the CNS-age oceanic basement to the west. If deformation at the BGA trough began with the onset of Bellingshausen plate motion, which we interpret as occurring at chron 33y (73.6 Ma) [Larter *et al.*, 2002], one would expect to see sedimentary layers deposited on its western flank before deformation (representing >10 Myr of accumulation), with an easterly component of dip which parallels that of the underlying basement. However, no such layers are seen, and so we infer that the BGA trough formed during, or soon after, the CNS. This suggests to us that initially the BGA trough could have accommodated MBL-ANP motion, which gave way to BEL-ANP motion with the development of an independent Bellingshausen plate at chron 33y [Larter *et al.*, 2002, Figures 7b and 8a]. Although we cannot readily account for the position or orientation of the BGA trough, we suspect that it developed along a preexisting lithospheric weakness such as a transform fault or abandoned spreading ridge. Severinghaus and Atwater [1990] have shown that microplates formed by fragmentation of a subducting plate may rotate, and thus produce ridge segments and transform faults in any orientation. This may explain the misalignment of the BGA trough with other tectonic structures in the Bellingshausen Sea. Cande *et al.* [1995] proposed that the Bellingshausen plate was itself captured by the Antarctic plate at chron 27 as part of a general plate reorganization in the South Pacific, which probably rendered the trough tectonically inactive by 61 Ma. However, recent data from the Adare Trough, off the western Ross Sea, have been

interpreted as indicating that Marie Byrd Land moved up to 180 km relative to East Antarctica during Eocene and Oligocene time [Cande *et al.*, 2000]. This raises the possibility that Marie Byrd Land might also have moved a small distance relative to the Antarctic Peninsula during the same interval. If such motion did occur during the mid-Tertiary, the BGA trough may have accommodated some of it.

4. Conclusions

[65] Marine geophysical data presented in this study provide new insights into the structure and tectonic evolution of the Pacific margin of Antarctica. Some specific findings are listed below.

1. New tectonic reconstructions [Larter *et al.*, 2002] show that the Bellingshausen Sea has a complex geological history involving interactions between the Pacific, Antarctic, Bellingshausen and Phoenix plates, and several short-lived microplates. These reconstructions, together with MCS and gravity profiles presented here, show that the CSGA and BGA correspond to relict plate boundaries, which were probably active during the Late Cretaceous and early Tertiary.

2. The CSGA corresponds to an acoustically opaque structural high buried beneath the Antarctic continental slope between 83 and 93°W. Results of gravity modeling suggest that this structure represents the top part of a deformed sediment wedge, which is probably underlain by oceanic basement. We interpret this body as a buried accretionary prism, which formed during southward subduction of the Phoenix and Charcot plates beneath the margin before Chatham Rise rifted from West Antarctica.

3. MCS profiles crossing the Antarctic Peninsula margin northeast of the CSGA show no evidence of an extensive buried accretionary prism, but instead reveal an abrupt northeastward steepening of the continental slope near 78°W. We attribute these changes in tectonic style and slope morphology, at least in part, to subduction erosion resulting from subduction of rough oceanic basement topography which formed at the slow spreading ANT-PHO ridge after chron C23r (52 Ma).

4. The BGA near 94°45'W corresponds to a buried asymmetric oceanic basement trough, where presumed CNS-age basement dips beneath more elevated basement to the east. The BGA lies between areas of ocean floor formed by PAC-MBL/PAC-BEL and ANT-PHO spreading. However, our new reconstructions [Larter *et al.*, 2002] suggest that the ocean floor directly adjacent to both flanks of the BGA probably formed by earlier PAC-CHA spreading. MCS profiles show that the BGA low coincides with a thick, deformed sediment wedge, and reveal two separate phases of tectonism; basement underlying the western trough flank was first tilted to the east, and then to the south. The timing and mode of formation of the BGA trough are uncertain, although it probably formed along a preexisting lithospheric weakness in the Charcot plate during the CNS. We suggest that the oceanic crust immediately east of the BGA trough formed as part of the Charcot plate, but subsequently became coupled to the Antarctic Peninsula, as a result of cessation of Charcot plate subduction along the nearby continental margin. In this way, deformation in the trough could have accommodated MBL-

ANP motion, which later gave way to BEL-ANP motion with the development of an independent Bellingshausen plate. We suspect that tectonism ceased at chron 27, as part of a general plate reorganization in the South Pacific. This reorganization included inception of ANT-PHO spreading at the DGGA [Larter et al., 2002].

[66] **Acknowledgments.** We thank the officers, crew and scientists who participated in RRS *James Clark Ross* and R/V *Polarstern* cruises for assistance in obtaining the original data, and Seymour Laxon (University College London) and Dave McAdoo (NOAA) for providing the ERS-1 marine gravity field. We also thank Dietmar Müller and two anonymous referees for their constructive reviews, and Joann Stock for providing unpublished data.

References

- Aubouin, J., J. Bourgois, and J. Azéma, A new type of active margin: the convergent-extensional margin, as exemplified by the Middle America Trench off Guatemala, *Earth Planet. Sci. Lett.*, *67*, 211–218, 1984.
- Ballance, P. F., D. W. Scholl, T. L. Vallier, A. J. Stevenson, H. Ryan, and R. H. Herzer, Subduction of a Late Cretaceous seamount of the Louisville Ridge at the Tonga Trench: A model of normal and accelerated tectonic erosion, *Tectonics*, *8*, 953–962, 1989.
- Barker, P. F., The Cenozoic subduction history of the Pacific margin of the Antarctic Peninsula: Ridge crest-trench interactions, *J. Geol. Soc. (London)*, *139*, 787–801, 1982.
- Bird, R. T., and R. A. Pockalny, Late Cretaceous and Cenozoic sea-floor and oceanic basement roughness: Spreading rate, crustal age and sediment thickness correlations, *Earth Planet. Sci. Lett.*, *123*, 239–254, 1994.
- Bonatti, E., M. Ligi, L. Gasperini, A. Peyve, Y. Raznitsin, and Y. J. Chen, Transform migration and vertical tectonics at the Romanche fracture zone, equatorial Atlantic, *J. Geophys. Res.*, *99*, 21,779–21,802, 1994.
- Bourgois, J., et al., Seabeam and seismic reflection imaging of the tectonic regime of the Andean continental margin off Peru (4°S to 10°S), *Earth Planet. Sci. Lett.*, *87*, 111–126, 1988.
- Cande, S. C., and D. V. Kent, Revised calibration of the geomagnetic polarity time scale for the Late Cretaceous and Cenozoic, *J. Geophys. Res.*, *100*, 6093–6096, 1995.
- Cande, S. C., E. M. Herron, and B. R. Hall, The early Cenozoic tectonic history of the southeast Pacific, *Earth Planet. Sci. Lett.*, *57*, 63–74, 1982.
- Cande, S. C., C. A. Raymond, J. Stock, and W. F. Haxby, Geophysics of the Pitman Fracture Zone and Pacific-Antarctic plate motions during the Cenozoic, *Science*, *270*, 947–953, 1995.
- Cande, S. C., J. M. Stock, R. D. Müller, and T. Ishihara, Cenozoic motion between East and West Antarctica, *Nature*, *404*, 145–150, 2000.
- Carlson, R. L., and G. S. Raskin, Density of the ocean crust, *Nature*, *311*, 555–558, 1984.
- Christensen, N. I., and W. D. Mooney, Seismic velocity structure and composition of the continental crust: A global view, *J. Geophys. Res.*, *100*, 9761–9788, 1995.
- Cochrane, G. R., and A. K. Cooper, Modeling of Cenozoic stratigraphy in the Ross Sea using sonobuoy seismic-refraction data, in *Recent Progress in Antarctic Earth Science*, edited by Y. Yoshida, K. Kaminuma, and S. Shiraiishi, pp. 619–625, Terra Sci., Tokyo, 1992.
- Cunningham, A. P., R. D. Larter, and P. F. Barker, Glacially prograded sequences on the Bellingshausen Sea continental margin near 90°W (abstract), *Terra Antarct.*, *1*, 267–268, 1994.
- Cunningham, A. P., R. D. Larter, P. F. Barker, K. Gohl, and F. O. Nitsche, Multichannel seismic investigation of the 'Bellingshausen Gravity Anomaly' and West Antarctic continental margin near 95°W, in *Antarctica at the Close of a Millennium: Proceedings of the 8th International Symposium on Antarctic Earth Sciences*, edited by J. A. Gamble, D. N. B. Skinner, and S. Henrys, *Bull. R. Soc. N. Z.*, *35*, 201–206, 2002.
- DeMets, C., and D. S. Wilson, Relative motions of the Pacific, Rivera, North American, and Cocos plates since 0.78 Ma, *J. Geophys. Res.*, *102*, 2789–2806, 1997.
- Dobrin, M. B., *Introduction to Geophysical Prospecting*, pp. 455–459, McGraw-Hill, New York, 1976.
- Gohl, K., F. Nitsche, and H. Miller, Seismic and gravity data reveal Tertiary interplate subduction in the Bellingshausen Sea, southeast Pacific, *Geology*, *25*, 371–374, 1997a.
- Gohl, K., F. O. Nitsche, K. Vanneste, H. Miller, N. Fechner, L. Oszko, C. Hübscher, E. Weigelt, and A. Lambrecht, Tectonic and sedimentary architecture of the Bellingshausen and Amundsen Sea basins, SE Pacific, by seismic profiling, in *The Antarctic Region: Geological Evolution and Processes, Proceedings of the 7th International Symposium on Antarctic Earth Sciences*, edited by C. A. Ricci, pp. 719–723, Terra Antarct. Publ., Siena, Italy, 1997b.
- Hagen, R. A., K. Gohl, R. Gersonde, G. Kuhn, D. Völker, and V. N. Kodagali, A geophysical survey of the De Gerlache Seamounts: preliminary results, *Geo Mar. Lett.*, *18*, 19–25, 1998.
- Hamilton, E. L., Sound velocity gradients in marine sediments, *J. Acoust. Soc. Am.*, *65*, 909–922, 1979.
- Herron, E. M., and B. E. Tucholke, Sea-floor magnetic patterns and basement structure in the southeastern Pacific, *Initial Rep. Deep Sea Drill. Proj.*, *35*, 263–278, 1976.
- Kimura, K., Geological and geophysical survey in the Bellingshausen Basin, off Antarctica, *Antarct. Rec.*, *75*, 12–24, 1982.
- Lallemant, S., and X. Le Pichon, Coulomb wedge model applied to subduction of seamounts in the Japan Trench, *Geology*, *15*, 1065–1069, 1987.
- Larter, R. D., and P. F. Barker, Seismic stratigraphy of the Antarctic Peninsula Pacific margin: A record of Pliocene-Pleistocene ice volume and paleoclimate, *Geology*, *17*, 731–734, 1989.
- Larter, R. D., and P. F. Barker, Effects of ridge crest-trench interaction on Antarctic-Phoenix spreading: Forces on a young subducting plate, *J. Geophys. Res.*, *96*, 19,583–19,607, 1991a.
- Larter, R. D., and P. F. Barker, Neogene interaction of tectonic and glacial processes at the Pacific margin of the Antarctic Peninsula, in *Sedimentation, Tectonics and Eustasy, Int. Assoc. Sedimentol. Spec. Publ.*, *12*, edited by D. I. M. Macdonald, pp. 165–186, Blackwell, Malden, Mass., 1991b.
- Larter, R. D., and A. P. Cunningham, The depositional pattern and distribution of glacial-interglacial sequences on the Antarctic Peninsula Pacific margin, *Mar. Geol.*, *109*, 203–219, 1993.
- Larter, R. D., M. Rebesco, L. E. Vanneste, L. A. P. Gambôa, and P. F. Barker, Cenozoic tectonic, sedimentary and glacial history of the continental shelf west of Graham Land, Antarctic Peninsula, in *Geology and Seismic Stratigraphy of the Antarctic Margin, part 2, Antarct. Res. Ser.*, vol. 71, edited by P. F. Barker and A. K. Cooper, pp. 1–27, AGU, Washington D. C., 1997.
- Larter, R. D., A. P. Cunningham, P. F. Barker, K. Gohl, and F. O. Nitsche, Structure and tectonic evolution of the West Antarctic continental margin and Bellingshausen Sea, *Korean J. Polar Res.*, *10*, 125–133, 1999.
- Larter, R. D., A. P. Cunningham, P. F. Barker, K. Gohl, and F. O. Nitsche, Tectonic evolution of the Pacific margin of Antarctica, 1, Late Cretaceous tectonic reconstructions, *J. Geophys. Res.*, *107*, 10.29/2000JB000052, in press, 2002.
- Ludwig, W. J., J. E. Nafe, and C. L. Drake, Seismic refraction, in *The Sea, Ideas and Observations in the Study of the Seas*, edited by A. E. Maxwell, pp. 53–84, John Wiley, New York, 1970.
- Mayes, C. L., L. A. Lawver, and D. T. Sandwell, Tectonic history and new isochron chart of the South Pacific, *J. Geophys. Res.*, *95*, 8543–8567, 1990.
- McAdoo, D. C., and S. Laxon, Antarctic tectonics: constraints from an ERS-1 satellite marine gravity field, *Science*, *276*, 556–560, 1997.
- McAdoo, D. C., and K. M. Marks, Gravity fields of the Southern Ocean from Geosat data, *J. Geophys. Res.*, *97*, 3247–3260, 1992.
- McCarron, J. J., and R. D. Larter, Late Cretaceous to early Tertiary subduction history of the Antarctic Peninsula, *J. Geol. Soc. (London)*, *155*, 255–268, 1998.
- Molnar, P., T. Atwater, J. Mammereckx, and S. M. Smith, Magnetic anomalies, bathymetry, and tectonic evolution of the South Pacific since the Late Cretaceous, *Geophys. J. R. Astron. Soc.*, *49*, 383–420, 1975.
- National Geophysical Data Center, *Marine Geophysical Trackline Data (GEODAS/TRACKDAS), Data Announcement 96-MGG-01*, Natl. Oceanogr. Atmos. Admin., Boulder, Colo., 1996.
- Nitsche, F. O., A. P. Cunningham, R. D. Larter, and K. Gohl, Geometry and development of glacial continental margin depositional systems in the Bellingshausen Sea, *Mar. Geol.*, *162*, 277–302, 2000.
- Nitsche, F. O., K. Gohl, K. Vanneste, and H. Miller, Seismic expression of glacially deposited sequences in the Bellingshausen and Amundsen Seas, West Antarctica, in *Geology and Seismic Stratigraphy of the Antarctic Margin, part 2, Antarct. Res. Ser.*, vol. 71, edited by P. F. Barker and A. K. Cooper, pp. 95–108, AGU, Washington, D. C., 1997.
- Prestvik, T., C. G. Barnes, B. Sundvoll, and R. A. Duncan, Petrology of Peter I Øy (Peter I Island), West Antarctica, *J. Volcanol. Geotherm. Res.*, *44*, 315–338, 1990.
- Sandwell, D. T., and W. H. F. Smith, Marine gravity-anomaly from Geosat and ERS-1 satellite altimetry, *J. Geophys. Res.*, *102*, 10,039–10,054, 1997.
- Severinghaus, J., and T. Atwater, Cenozoic geometry and thermal state of the subducting slabs beneath North America, in *Basin and Range extensional tectonics near the latitude of Las Vegas, Nevada*, edited by B. P. Wernicke, pp. 1–22, GSA, Boulder, Colo., 1990.

- Stock, J., and P. M. Molnar, Revised history of early Tertiary plate motion in the south-west Pacific, *Nature*, 325, 495–499, 1987.
- Tucholke, B. E., Sedimentation processes and acoustic stratigraphy in the Bellingshausen Basin, *Mar. Geol.*, 25, 209–230, 1977.
- Tucholke, B. E., and R. E. Houtz, Sedimentary framework of the Bellingshausen Basin from seismic profiler data, *Initial Rep. Deep Sea Drill. Proj.*, 35, 197–228, 1976.
- Vanneste, L. E., and R. D. Larter, Sediment subduction, subduction erosion and strain regime in the northern South Sandwich forearc, *J. Geophys. Res.*, 107(B7), 10.1029/2001JB000396, 2002.
- von Huene, R., and D. W. Scholl, Observations at convergent margins concerning sediment subduction, subduction erosion, and the growth of continental crust, *Rev. Geophys.*, 29, 279–316, 1991.
- Weissel, J. K., D. E. Hayes, and E. M. Herron, Plate tectonic synthesis: the displacements between Australia, New Zealand, and Antarctica since the Late Cretaceous, *Mar. Geol.*, 25, 231–277, 1977.
- White, R. S., R. K. O’Nions, and D. McKenzie, Oceanic crustal thickness from seismic measurements and rare earth element inversions, *J. Geophys. Res.*, 97, 19,683–19,715, 1992.
-
- P. F. Barker and R. D. Larter, British Antarctic Survey, High Cross, Madingley Road, Cambridge CB3 0ET, UK. (p.barker@bas.ac.uk; r.larter@bas.ac.uk)
- A. P. Cunningham, ARK CLS Limited, Mill Court, Featherstone Rd., Wolverton Mill South, Milton Keynes MK12 5EU, UK. (alex.cunningham@arkcls.com)
- K. Gohl, Alfred Wegener Institute for Polar and Marine Research, P.O. Box 120161, D27515 Bremerhaven, Germany. (kgohl@awi-bremerhaven.de)
- F. O. Nitsche, Lamont-Doherty Earth Observatory of Columbia University, Rte. 9W, Palisades, NY 10964, USA. (fnitsche@ldeo.columbia.edu)